Acta Biomaterialia 15 (2015) 39–47

Contents lists available at ScienceDirect

Acta Biomaterialia

journal homepage: www.elsevier.com/locate/actabiomat

Photosynthetic biomaterials: A pathway towards autotrophic tissue engineering

Thilo Ludwig Schenck [a,1], Ursula Hopfner [a,1], Myra Noemi Chávez [a,1], Hans-Günther Machens [a], Ian Somlai-Schweiger [b], Riccardo Enzo Giunta [a,c], Alexandra Viola Bohne [d], Jörg Nickelsen [d], Miguel L. Allende [e], José Tomás Egaña [a,e,*]

[a] Department of Plastic Surgery and Hand Surgery, University Hospital rechts der Isar, Technische Universität München, Germany
[b] Department of Nuclear Medicine, University Hospital rechts der Isar, Technische Universität München, Germany
[c] Handchirurgie, Plastische Chirurgie, Ästhetische Chirurgie der Ludwig-Maximilians Universität München, Germany
[d] Molekulare Pflanzenwissenschaften, Biozentrum Ludwig-Maximilians-Universität München, Planegg-Martinsried, Germany
[e] FONDAP Center for Genome Regulation, Faculty of Science, Universidad de Chile, Santiago, Chile

ARTICLE INFO

Article history:
Received 27 August 2014
Received in revised form 2 December 2014
Accepted 15 December 2014
Available online 20 December 2014

Keywords:
Photosynthesis
Chlamydomonas reinhardtii
Biomaterials
Tissue engineering
Hypoxia

ABSTRACT

Engineered tissues are highly limited by poor vascularization *in vivo*, leading to hypoxia. In order to overcome this challenge, we propose the use of photosynthetic biomaterials to provide oxygen. Since photosynthesis is the original source of oxygen for living organisms, we suggest that this could be a novel approach to provide a constant source of oxygen supply independently of blood perfusion. In this study we demonstrate that bioartificial scaffolds can be loaded with a solution containing the photosynthetic microalgae *Chlamydomonas reinhardtii*, showing high biocompatibility and photosynthetic activity *in vitro*. Furthermore, when photosynthetic biomaterials were engrafted in a mouse full skin defect, we observed that the presence of the microalgae did not trigger a native immune response in the host. Moreover, the analyses showed that the algae survived for at least 5 days *in vivo*, generating chimeric tissues comprised of algae and murine cells. The results of this study represent a crucial step towards the establishment of autotrophic tissue engineering approaches and suggest the use of photosynthetic cells to treat a broad spectrum of hypoxic conditions.

1. Introduction

The optimal three-dimensional restoration of injured tissues requires templates to guide the growth of cells. These artificial templates are known as scaffolds and their improvement is a major task in the field of regenerative medicine [1]. It is commonly accepted that a major problem that causes clinical failure of these scaffolds is their delayed vascularization [2], which results in lack of proper blood perfusion with the necessary cells, nutrients and especially oxygen. Despite great efforts to circumvent this problem through the development of new technologies and biomaterials [1,3,4], autologous tissue transplantation remains the gold standard procedure to treat the vast majority of complex tissue defects, and the use of scaffolds is limited to cases where autologous tissue is not available.

Oxygen is a key molecule involved in many physiological processes and is particularly important during wound healing and tissue repair. In this regard, strong evidence demonstrates that oxygen is involved in almost every step of the tissue healing process. In fact, preclinical and clinical data strongly support the observation that wound healing is impaired by insufficient oxygen supply [5]. Among other functions, oxygen is required in wounds to maintain energy supply (ATP levels) of the newly growing tissue and for the correct deposition and polymerization of collagen fibers [6]. Oxygen is also needed for the generation of reactive oxygen species, which act as signaling molecules and play a key role preventing wound infections by depleting bacteria through oxidation. The importance of oxygen as a key mediator promoting wound healing has been addressed in several review articles [7–10]. Moreover, as a product of anaerobic metabolism, the accumulation of lactic acid causes additional toxicity in hypoxic tissues [11,12].

Common approaches to enhance vascularization in scaffolds include the use of recombinant pro-angiogenic growth factors

* Corresponding author at: Department Plastic Surgery and Hand Surgery, University Hospital rechts der Isar, Technische Universität München, Ismaningerstr. 22/81675 Munich, Germany. Tel.: + 49 89 4140 7510; fax: + 49 89 4140 7515.
E-mail address: tomasega@gmail.com (J.T. Egaña).
[1] These authors contributed equally to this work.

http://dx.doi.org/10.1016/j.actbio.2014.12.012
1742-7061/

[13], gene vectors encoding for therapeutic molecules [14] and stem cells, which may contribute to vascularization by direct differentiation into vascular structures [15] or through the secretion of paracrine factors [16]. All these approaches are promising in accelerating vascularization, but even under optimal conditions, re-establishment of proper oxygen levels through vascular supply requires several days or weeks.

The approach presented here, named HULK (from the German abbreviation of Hyperoxie Unter Licht Konditionierung), aims at generating chimerical tissues containing photosynthetic cells to provide a local source of oxygen, through a mechanism independent of blood perfusion: photosynthesis. In this work we evaluated the behavior of photosynthetic scaffolds after *in vivo* transplantation. As a proof of concept, in this study we combined the photosynthetic, unicellular microalgae *Chlamydomonas reinhardtii* with a collagen-based template, generating a photosynthetically activated scaffold for dermal wound repair.

2. Material and methods

2.1. Cell culture of C. reinhardtii

Cell-wall deficient *C. reinhardtii* strain UVM4-GFP [17] was grown photomixotrophically in liquid TAPS-medium (Tris-Acetate-Phosphate supplemented with 1% (w/v) sorbitol) [18] under continuous white light exposure (1500 lux). Cell concentration in the culture was determined using a Casy Counter TT (Roche Diagnostics, Mannheim, Germany).

2.2. Cell seeding in the scaffolds

For *in vitro* experiments, if not stated otherwise, Integra matrix single layer (IM, Integra Life Science Corporation, Plainsboro, NJ, USA) was used as a scaffold. For seeding of *C. reinhardtii*, the algae suspension was mixed with fibrinogen (Tissuecol-Kit 2.0 Immuno, Baxter GmbH, Unterschleißheim, Germany) in a 1:1 ratio to the respective final concentration. Pieces of IM (12 mm diameter) were cut using a biopsy punch and dried with sterile gauze. 50 µl thrombin solution followed by 100 µl of the algae–fibrinogen solution were pipetted over each scaffold. Control scaffolds were prepare as HULK but only with algae medium (TAPS). After 1 h, the scaffolds were covered with TAPS-medium and incubated over the desired period of time at room temperature and constant illumination (1500 lux). Pictures of the scaffolds were taken with a stereomicroscope (Stemi 2000-C, Carl Zeiss AG, Oberkochen, Germany).

2.3. Scanning electron microscopy

Scaffolds were seeded with 1×10^4 *C. reinhardtii* cells as described above and incubated for 4 days at room temperature under a constant white light exposure (1500 lux). After fixation in 3% glutaraldehyde and dehydration with graded ethanol, samples were air-dried and sputtered with 20 nm gold (Baltec, SCD 005; Leica Microsystems, Wetzlar, Germany). An acceleration voltage of 5 kV was used for the scanning electron microscopy analysis (Hitachi, S-3500-N, Tokyo, Japan).

2.4. Chlorophyll measurements

Scaffolds were seeded with 3×10^5 *C. reinhardtii* cells as described above. At different culture times (days 1 and 7) the scaffolds were placed in 500 µl dimethyl sulfoxide (DMSO, Sigma, St Louis, MO) and shock frozen in liquid nitrogen. Afterwards samples were defrosted and additional 500 µl DMSO was added to each sample. Next, scaffolds were mechanically disrupted with a pestle and the optical density was measured at 435 nm (Nanodrop, Thermo Scientific, Waltham, MA, USA).

2.5. Oxygen release measurements

Scaffolds were seeded at a final concentration of 2.5×10^6 cells per scaffold and incubated for 3 days at room temperature, followed by a 16 h incubation in the dark prior to the start of the measurement. Afterwards, samples were placed under hypoxic conditions (1% oxygen) and oxygen concentrations *in vitro* were constantly measured by the SensorDish Reader (PreSens Gmbh, Regensburg, Germany) in Oxodishes according to the manufacturer's instructions. For light stimulation a lamp with the full spectrum of white light (Nano Light, 11 W, Dennerle, Vinningen, Germany) was placed 40 cm from the sample providing ~1500 lux. Oxygen concentration was recorded and measurements stopped once saturation of the system ($\geqslant$50% pO_2) had been maintained for 1 h.

2.6. Full-skin defect model

For the *in vivo* experiments, scaffolds were prepared as for the oxygen release measurements but in this case we used a double-layered scaffold where the collagen is covered with a silicone layer on top, which acts as a temporary epidermis (Integra® DRT, Integra Life Science Corporation, Plainsboro, NJ, USA). Before implantation, HULK and control scaffolds were incubated in TAPS-medium for 3 days at room temperature and exposed to continuous white light (1500 lux). All procedures on laboratory animals were approved by the District Government of Upper Bavaria (Regierung von Oberbayern) and performed according to the current German animal welfare act (TierSchG). Experiments were performed on female nu/nu mice aged 6–8 weeks and with body weights of 20–25 g (Charles River, Sulzfeld, Germany). Under inhalative anesthesia (Isoflurane, Baxter Germany, Unterschleissheim, Germany), a bilateral 10 mm full-skin defect was created as we have described before [19]. Control and HULK scaffolds were implanted and covered with a transparent dressing (V.A.C.® Drape, KCI Medical Products, Wimborne Dorset, UK). In order to trigger the oxygen production, cages were equipped with a flexible LED module (20 V, 14.4 W, WW, 2700 K, Ledxon, Landshut, Germany) to stimulate the photosynthetic scaffolds with additional 3500 lux during daytime. According to the TierSchG, animals must be subjected to circadian cycles of 12/ 12 h light/darkness. Thus, photosynthetic implants could not be exposed for more than 12 h to light stimulation per day. Control animals were kept under the same light stimulation conditions. At day 5 post-transplantation, animals were euthanized by overdoses of anesthetics and the skin from the back, including the scaffolds, was excised for further analysis. Immune organs (spleen and lymph nodes) were removed and their size and weight were measured and related to their body weight. Whole blood was collected directly from the heart and allowed to clot by leaving it undisturbed on ice for 1 h. The clot was removed by centrifugation at 2000*g* for 10 min at 4 °C. Serum was transferred into a clean test tube and stored at −80 °C for further analysis. Six animals (12 scaffolds) per group were used in this study.

2.7. Histological analysis

Five days post-implantation, scaffolds were removed from the animals and fixed in 3.7% formaldehyde for 24 h at 4 °C. Afterwards samples were shock frozen in Tissuetec (Sakura, Alphen an den Rijn, the Netherlands) and sections of 20 µm thickness were prepared, stained and mounted in DAPI-Prolong-Gold (Invitrogen, Carlsbad, CA). Finally, pictures were taken with a fluorescence

microscope (Axio Observer, Carl Zeiss AG, Oberkochen, Germany) or an inverted phase-contrast microscope (Axiovert 25, Carl Zeiss AG) and analyzed with the Axiovision software (Carl Zeiss AG).

2.8. Viability of the algae in vivo

In order to evaluate the metabolic activity of the algae after transplantation, 3 and 5 days after implantation scaffolds were removed and stored at −80 °C in RNAlater (Qiagen, Hilden, Germany). After homogenization with a pestle, total RNA isolation was performed with a High Pure RNA Isolation Kit (Roche Applied Science GmbH, Mannheim, Germany). For reverse-transcription polymerase chain reaction (RT-PCR) a Transcriptor One Step RT-PCR Kit (Roche Applied Science GmbH, Mannheim, Germany) was used to determine the expression of the algal *psbD* gene. Primer sequences for *psbD* were: 5′-GCCGTAGGGTTGAATG-3′ and 5′-GTTGGTGTCAACTTGGTGG-3′. Mouse β-actin was used as a housekeeping gene: 5′-AGCCATGTACGTAGCCATCC-3′ and 5′-TCTCAGCTGTGGTGGTGAAG-3′.

2.9. Viability of the algae ex vivo

Biopsies of the explanted scaffold were taken (∼12 mm × 1 mm) and incubated for 24 h in liquid TAPS-medium supplemented with 10 μg ml^{-1} paromomycin. Next, samples were centrifuged (290*g*, 5 min) and cultured for 2 weeks in TAPS-agar plates containing the same concentration of antibiotics.

2.10. Cytokine protein array profile

Protein extracts were obtained by mechanical disruption as described above. A mouse cytokine panel-A protein array was performed using both the scaffold lysates and serum following the manufacturer's instructions (R&D Systems, Minneapolis, MN).

2.11. Zebrafish model of inflammatory response

Zebrafish (*Danio rerio*) embryos of the transgenic strain Tg (mpeg:EGFP [20]) were obtained from our laboratory-breeding colony. All embryos were collected by natural spawning and raised at 28.5 °C in E3 medium (5 mM NaCl, 0.17 mM KCl, 0.33 mM $CaCl_2$, 0.3 mM $MgSO_4$ equilibrated to pH 7.0); egg water was changed daily. Animals were anesthetized with MS-222 (Tricaine, A5040, Sigma, St Louis, MO) before each experiment. Embryonic ages are expressed in days-post-fertilization (dpf). *Escherichia coli* constitutively expressing red fluorescent protein [21] was grown in standard Luria Bertani (LB) medium supplemented with 50 μg ml^{-1} kanamycin. Cells used for the infection of zebrafish embryos were freshly grown overnight on LB, washed once by centrifugation (8000 rpm, 5 min) and suspended in TAPS-medium to a final concentration of 5×10^5 cells μl^{-1}. *C. reinhardtii* cells were suspended to the same concentration in fresh TAPS-medium. Both bacterial and algae suspensions were loaded into glass capillary needles. Using a microinjector (Microinjector MPPI-2 Pressure Injector, ASI), previously dechorionated zebrafish embryos of 3 dpf were injected with 1 nl of the respective cell suspension into the otic vesicle. Control injections with TAPS-medium were performed following the same protocol. Embryos were incubated for 4 h in E3 medium at 28 °C and imaged as described below. All procedures complied with guidelines of the Animal Ethics Committee of the University of Chile.

2.12. Confocal microscopy, fluorescence microscopy and image processing

Living zebrafish embryos were examined using an epifluorescence-inverted microscope (Olympus scan, Olympus Biosystems, Munich, Germany), equipped with a motorized stage. Embryos were chosen randomly, anesthetized and mounted in 0.75% low-melting-point agarose containing 5% Tricaine (Sigma, St Louis, MO) in a 35 mm imaging dish and fixed to a lateral position. Z-stack images of the otic vesicles were taken at a fixed distance of 10 μm between the planes. For image analysis, bright field and red fluorescence channels were used to locate and delineate the site of injection, whereas the number of recruited macrophages was obtained using only the images obtained in the green channel. Co-localization of red and green was the criterion used to determine phagocytosis. Z-stacks were taken with an average distance of 15 μm between the planes in a confocal microscope (Zeiss LSM 510 Meta, Carl Zeiss AG, Oberkochen, Germany). Merged projections of the frames were then used to generate a mosaic image of the whole fish using the software Image J.

2.13. Measurement of serum immunoglobulins

The concentrations of the mouse IgG and IgM in serum were determined by the specific *in vitro* enzyme-linked immunoabsorbent assays IgG Mouse Elisa Kit (ab151276, Abcam plc, Cambridge, UK) and IgM Mouse ELISA Kit (ab1330057, Abcam plc, Cambridge, UK), respectively, following the manufacturer's instructions.

2.14. Statistical analysis

All assays were repeated in at least three independent experiments. Data was expressed as mean ± SEM. Two-tailed Student's *t*-test was used to compare differences between two groups. GraphPad Prism 5 software (GraphPad Software, La Jolla, CA) was used for statistical analyses. Differences among means were considered significant when $P \leqslant 0.05$.

3. Results

3.1. Photosynthetic activation of the scaffolds

We have recently shown that algae can be directly incorporated in a collagen scaffold *in vitro* [22]. In contrast to this work, this time we followed a different approach by incorporating the algal cells using a biocompatible hydrogel as carrier [23]. The use of fibrin allows the cells to be kept on site and decreases the potential immune response to the algae. Both algae and fibrin were homogeneously distributed throughout the entire scaffold, penetrating even into the deepest layers of the material (Fig. 1A). The interaction of the fibrin–algae solution with the scaffold was further evaluated by scanning electron microscopy. Results showed that *C. reinhardtii* was found to be attached to the walls of the scaffold, forming cluster-like structures embedded in fibrin (Fig. 1B). Next, fibrin containing low densities of *C. reinhardtii* cells (3×10^5 cells per scaffold) were incorporated into the scaffolds. An increase of the algae-specific green color was observed over the scaffold and chlorophyll quantification revealed a significant increase from day 1 to day 7 ($P \leqslant 0.001$) (Fig. 2A). Under light stimulation, the oxygen released from the photosynthetic composite was quantified and compared between days 1 and 7. When placed in a hypoxic incubator (1% oxygen) a decrease in the pO_2 was always observed in the control group and was maintained throughout the experiment at levels of ∼1% pO_2 (data not shown). In the case of scaffolds seeded with algae and cultured for 1 day, ∼5 days

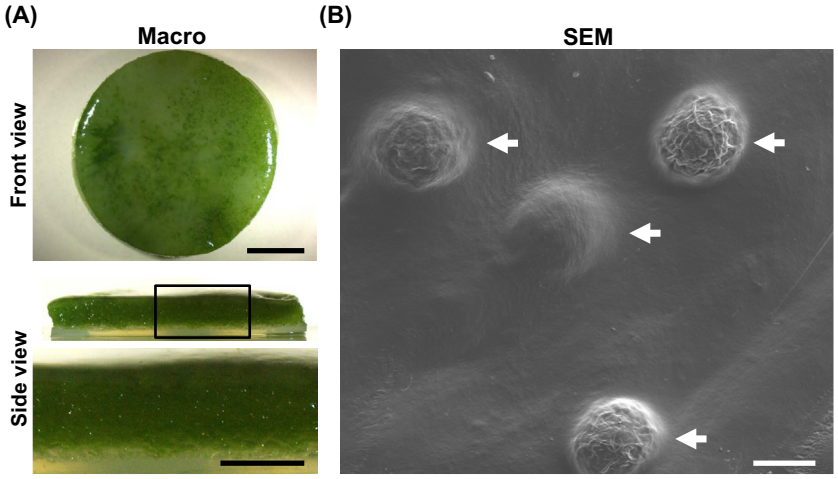

Fig. 1. Seeding of microalgae in the scaffold. Fibrin-containing *C. reinhardtii* was incorporated in a collagen scaffold and incubated in TAPS-medium for 3 days at room temperature and exposed to continuous white light (1500 lux). The overall green color shows that the fibrin–algae solution was homogeneously distributed in the scaffold (A, upper). A cross-section of the seeded material shows that the algae penetrate into the deepest layers of the scaffold (A, lower). SEM analysis showed that fibrin–algae solution covered the walls of the scaffold and that the microalgae grew on them forming fibrin-embedded photosynthetic clusters (B). Scale bar represents 2.5 mm in A upper, 1 mm in A lower and 25 μm in B.

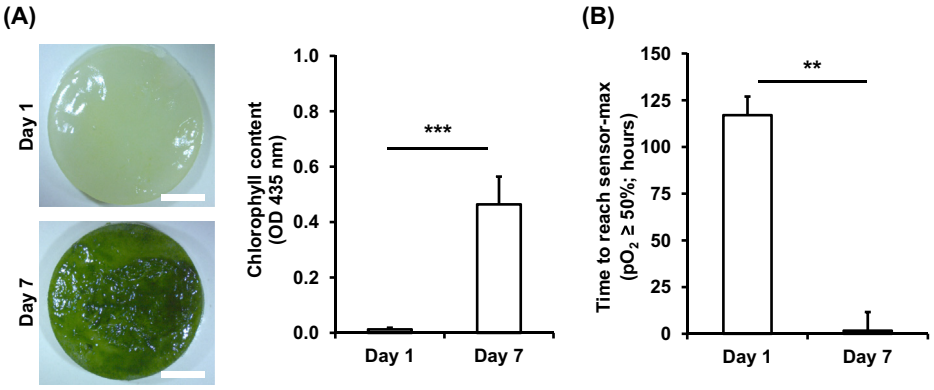

Fig. 2. Proliferative and photosynthetic capacity of microalgae in the scaffold. Seven days after seeding the algae in low density, significant increases of the total chlorophyll content (A) and oxygen release were observed in the scaffolds (B). While values for the control group were stable at ~1% pO_2, photosynthetic scaffolds reached saturation of the oxygen sensor ($pO_2 \geqslant 50\%$). The time to reach saturation was significantly reduced by proliferation of the algae (B). Scale bar represents 2.5 mm in A. $^{**}P \leqslant 0.005$; $^{***}P \leqslant 0.001$; $n \geqslant 3$. Results are shown as mean + SD.

(117 ± 8.33 h) were needed to reach saturation of the oxygen sensor ($pO_2 \geqslant 50\%$). In contrast, when the algae were previously cultured for 7 days in the scaffolds, a saturation time of <2 h (1.67 ± 0.33 h) was required (Fig. 2B), confirming an increased photosynthetic activity due to cell proliferation.

3.2. Engraftment of photosynthetic scaffolds in vivo

Our next goal was to evaluate the feasibility of photosynthetic biomaterials *in vivo*. Bilateral full-skin defects were created in the back of athymic nude mice and either control or HULK scaffolds replaced the removed tissue. No major complications were observed during or after the operative procedure. At 5 days post-transplantation, no macroscopic signs of infection or foreign body reaction were observed in the wound area in either of the groups and we did not observe significant differences in the body weight of either animal group. In the control group animals showed an average weight of 0.97 ± 0.04% vs. their body weight prior to the implantation, which had no statistical significance compared to HULK, where the average was 0.94 ± 0.06% (Fig. 6). The appearance of a representative animal is shown at 5 days post-operation (Fig. 3). In order to determine the presence of infiltrating vessels, scaffolds were removed and visualized by transillumination. The results showed that the presence of the algae does not hinder vascularization of the scaffold *in vivo* (Fig. 3).

3.3. Ex vivo analysis of C. reinhardtii

In order to evaluate the distribution of the algae in the regenerating tissue, cryosections were performed at day 5 post-transplantation, revealing that the algae exhibit a normal shape as well as color and distribute along the whole scaffold (Fig. 4A and B). Further efforts to evaluate the viability of *C. reinhardtii in vivo* led us to investigate mRNA isolated from photosynthetic biomaterials harvested at days 3 and 5 post-transplantation, and RT-PCR analysis was performed to detect the algae-specific, chloroplast *psbD* mRNA (encoding the photosystem II reaction center protein D2). The result of the RT-PCR analysis showed that *psbD* mRNA can be detected in the wound area for at least 5 days post-transplantation (Fig. 4A and C), suggesting that algae were metabolically active in the scaffold. This result was confirmed by outgrowing experiments where algae were capable of growing colonies from six different wound biopsies obtained 5 days post-implantation (Fig. 4D).

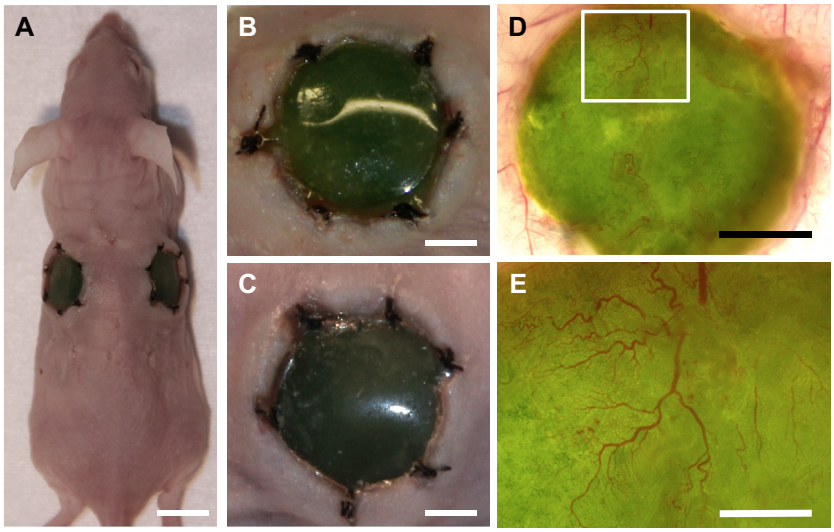

Fig. 3. Engraftment of photosynthetic scaffolds *in vivo*. Collagen scaffolds seeded with the algae were engrafted in a bilateral full-skin defect, remaining green for 5 days *in vivo* (A). A close up of the left (B) and right (C) implant shows no macroscopic signs of infection or inflammation at the wound area. A detailed analysis of the implanted biomaterial showed high vascularization levels in the presence of microalgae (D–E). Scale bar represents 1 cm in A, 4 mm in B–D and 1 mm in E. Results were obtained for at least eight independent experiments.

3.4. Local and systemic inflammatory response to photosynthetic biomaterials

Algae and endogenous cells were visualized histologically in order to gain more detailed insight on their interaction (Fig. 5A). At 5 days post-implantation, an algae-mammalian chimeric tissue was observed in the wound area (Fig. 5A). It is important to notice that although athymic nude mice present impaired T-cell-mediated response, the innate immune system is fully functional in this model. To test whether algal cells trigger an inflammatory response in the wound, we performed an inflammatory cytokine profiler array on protein extracts obtained from scaffolds explanted 5 days after surgery (Fig. 5B). No significant differences were observed in the levels of molecules related to the recruitment of immunoactive cells such as the chemokine (C-X-C motif) ligands 1, 2, 9, 10, 13 and the chemokine (C-C motif) ligands 1–5. Moreover, the presence of *C. reinhardtii* did not trigger the expression of other molecules primarily described as key regulators of the immune response, such as IFN-γ or the interleukins: 2, 3, 4, 5, 7, 10, 12, 13, 17, 23 and 27 (Fig. 5B). Overall, among the 40 analyzed cytokines, the levels of only two molecules, C5a and CCL12, significantly increased in HULK when compared to the control group ($P \leqslant 0.05$; Fig. 5B).

In addition, systemic inflammatory effects of photosynthetic materials were further evaluated by dissecting spleen and lymph nodes (mesenteric (MLN) and iliac (ILN)) at day 5 and comparing their sizes to those of the control animals (Fig. 6). For spleen, values of 0.45 ± 0.07% and 0.37 ± 0.08% were observed for the control and HULK groups, respectively. Similar results were obtained for MLN and ILN where values of 0.01 ± 0.003% and 0.03 ± 0.004% were observed respectively in the control group, while values of 0.01 ± 0.001% and 0.04 ± 0.006% were detected in HULK (Fig. 6A). Similarly, no statistical differences were observed on the weight loss between the groups, which compared to the weight before the operation showed values of 96.7 ± 3.7% for the control group and 94.0 ± 6.2% for HULK (Fig. 6B). Additionally we also evaluate the systemic immune response by measuring the concentration of immunoglobulin M and G (IgM and IgG) in serum, as well as the levels of the 40 inflammatory cytokines described above. Results showed concentrations of 116.0 ± 92.2 mg IgG ml^{-1} and 181.5 ± 57.8 mg IgM ml^{-1} for the control group and values of 89.2 ± 19.4 mg IgG ml^{-1} and 206.2 ± 92.5 mg IgM ml^{-1} were detected in HULK (Fig. 6C). Thus, no significant differences were observed in either the concentrations of immunoglobulins or their ratio to each other (2.2 ± 0.9 for control and 2.3 ± 0.7 for HULK). Finally, results obtained with the cytokine array detected the presence of the cytokines C5a, CCL1, CCL12, CD54, M-CSF and TIMP-1 in both groups but no statistical differences among control and HULK (Fig. 6D). In conclusion, no striking differences in the immune response between HULK and control mice were detected.

Because the low inflammatory response to *C. reinhardtii* described above could be due the high inflammatory background of the normal wound healing process and also by the fibrin encapsulation of the algae, we decided to challenge the innate immune response to *C. reinhardtii* in a second, well-established *in vivo* model. Therefore, microalgae were injected in the otic cavity of transgenic zebrafish larvae, expressing green fluorescent protein (GFP) in macrophages (Fig. 7A, top). Macrophage activity was then compared to animals injected with only medium as Control or a suspension of *E. coli* cells expressing red fluorescent protein (RFP; Fig. 7A, bottom). Whereas no differences were observed to the control group, the number of macrophages infiltrating the area injected with *C. reinhardtii* was significantly lower than in the group injected with *E. coli* (Fig. 7B; $P \leqslant 0.05$). Additionally, from the examination of infiltrating phagocytes in each case, we observed that in those fish injected with *E. coli* the number of double positive labeled phagocytes (i.e. phagocytic macrophages) was significantly higher than in the *C. reinhardtii* group (Fig. 7C; $P \leqslant 0.001$). These observations suggest that the immune response to *C. reinhardtii* is drastically reduced as compared to infectious bacteria.

4. Discussion

Hypoxia is broadly recognized as one of the main problems limiting the progress of tissue engineering [24], thus several approaches have been implemented in order to improve oxygenation *in vitro* and *in vivo*. For instance, artificial oxygen carriers, such as perfluorocarbon or modified hemoglobin, have been used to increase oxygen transport and transfer within biomaterials [25]. However, their use is associated with systemic side effects such

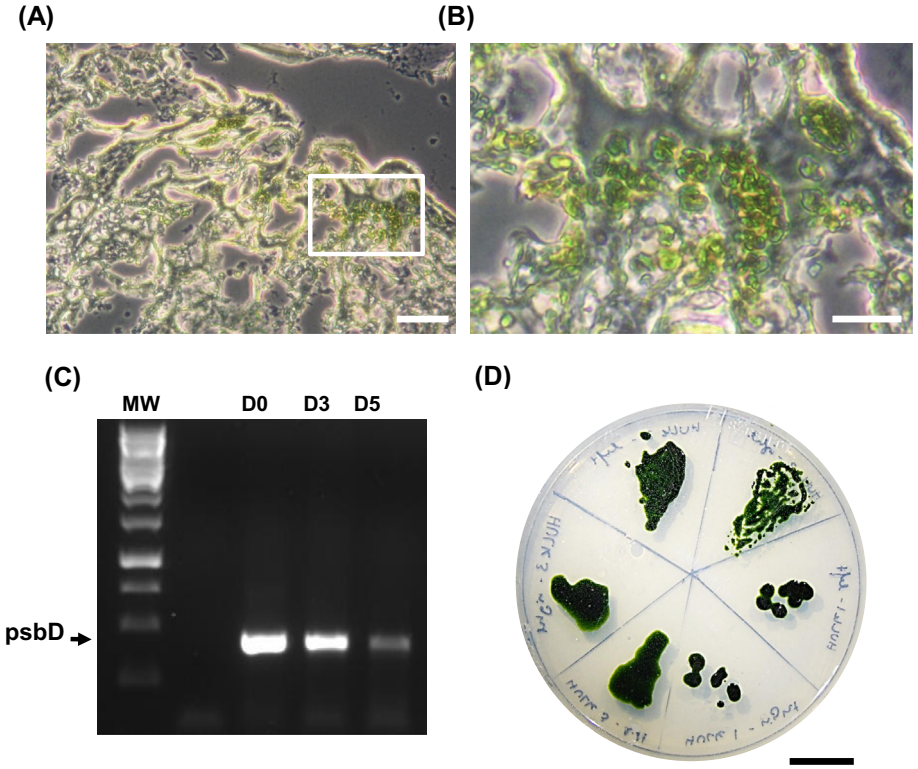

Fig. 4. Survival of the microalgae after transplantation. Five days post-transplantation the microalgae seem to be intact and equally distributed in the scaffold (A-B). RT-PCR analysis was performed to determine the presence of *psbD* mRNA at days 0, 3 and 5 (C). Finally, viability of the algae *in vivo* was confirmed by their capability to be regrown out of six different wound biopsies taken at day 5 post-implantation (D). Scale bar represents 50 μm in A, 20 μm in B and 2 cm in D. Results were obtained for at least six independent experiments.

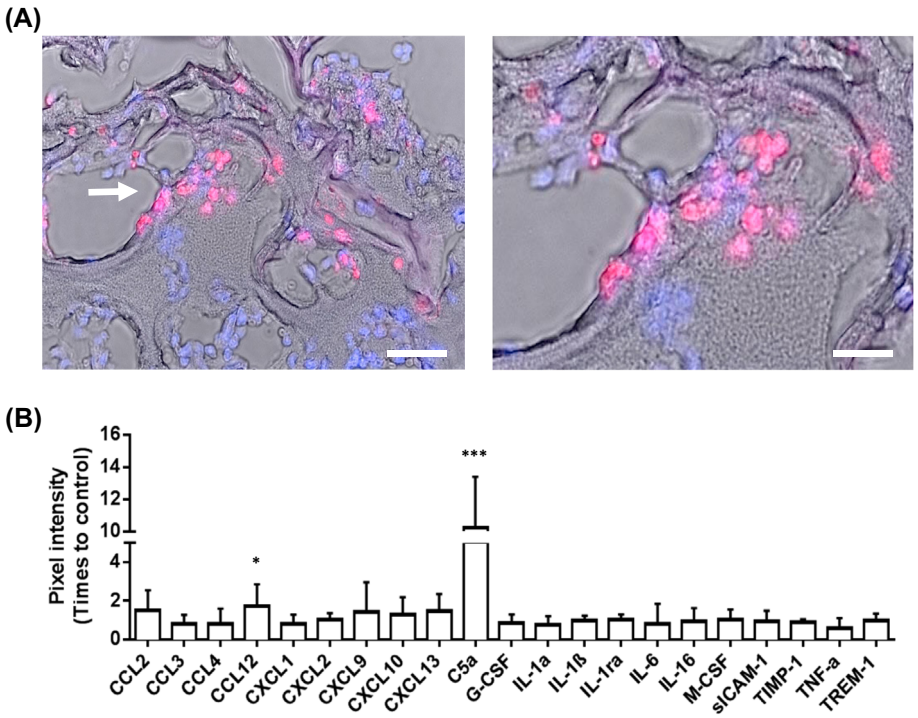

Fig. 5. Ex vivo analysis of photosynthetic biomaterials. Five days post-transplantation scaffolds were removed and analyzed. Histological sections show the formation of chimeric tissues composed of photosynthetic (red, chlorophyll autofluorescence) and mouse cells (blue, DAPI) (A). The white arrow shows the area zoomed in the left picture. An inflammatory cytokine protein array was performed over protein extracts. Among the 40 analyzed cytokines, the levels of only two molecules, C5a and CCL12, were significantly increased in the wound area of HULK compared to the control group (B). Scale bar represents 50 μm in A left and 20 μm A right. Results are shown as mean + SD.

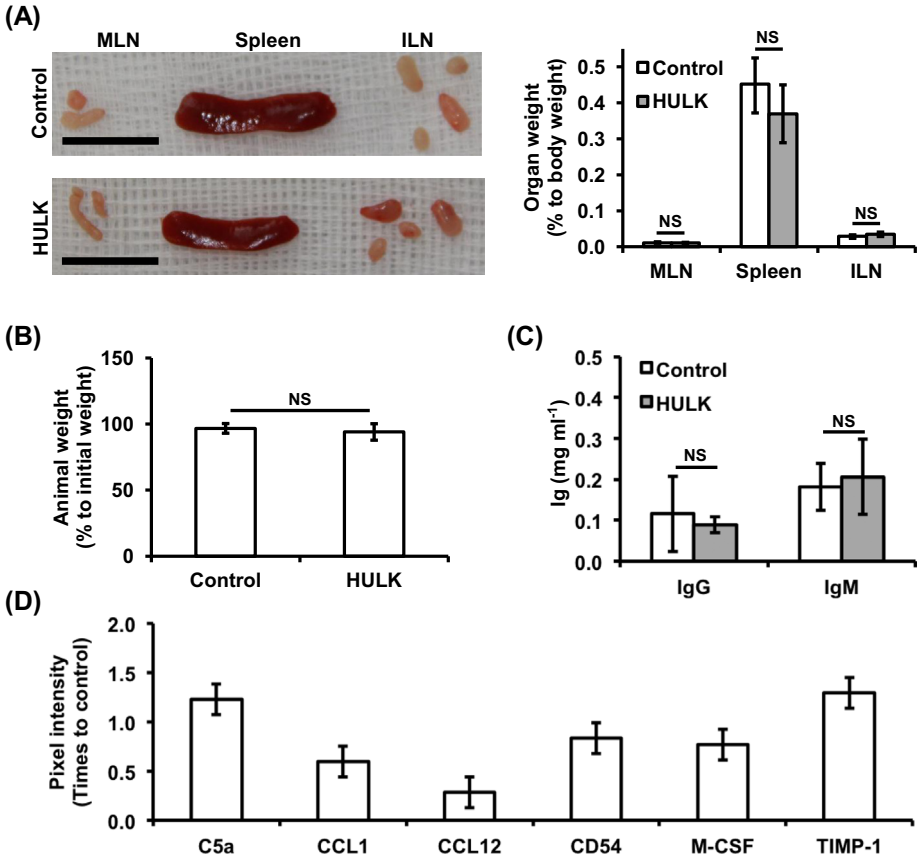

Fig. 6. Systemic effects of implanting photosynthetic biomaterial. Five days post-transplantation no significant differences were detected among the groups in the size of the immune organs (spleen and lymph nodes; A). The weight loss of the animals did not differ between the two groups (B). Quantification of immunoglobulins G (IgG) and M (IgM) did not show any variation between the control and HULK groups (C). Cytokines C5a, CCL1, CCL12, CD54, M-CSF and TIMP-1 were equally present in the serum of animals regardless the experimental group (D). Scales bar represents 1 cm in A. Results are shown as mean ± SD.

as vasoconstriction [26–28] and the toxic build-up of compounds due to failure of metabolic removal [28]. Another interesting approach has been the development of biomaterials containing solid sodium percarbonate that releases oxygen upon its chemical decomposition [29], yet these materials raise concerns about intermediate hydrogen peroxide generation and residuals. In contrast to those approaches, photosynthetic biomaterials may provide an unlimited source of oxygen, which merely depends on light stimulation. By introducing an alternative oxygen source to blood perfusion, difficulties related to graft thickness or survival after implantation could be easier to overcome. Furthermore, the photosynthetic release of oxygen from the construct itself may also hamper anaerobic bacteria infections. Finally, such an approach benefits from transiency, meaning that once the tissue is well vascularized and the algae are no longer needed, photosynthetic cells could be eliminated from the recipient if required by, for instance, light deprivation of the wound area, the use of gene-modified algae strains or the local application of non-toxic herbicides.

The use of fibrin in this procedure plays an important role for keeping the algal cells on site after transplantation (Fig. 1A, B). It also provides a highly compatible matrix for cell proliferation and oxygen release (Fig. 2A, B). Compared to control scaffolds, the saturation curve observed in HULK showed an increase in the pO_2 of at least 50 times, which is far above the increase observed in previous attempts, where barely 0.2 times more oxygen were achieved [29,30]. Although such a boost of the pO_2 could be potentially considered as toxic, it is important to mention that photosynthetic production of oxygen is directly associated with the number of algae and with the light intensity applied to the scaffolds [22]. Thus, a feasible approach to modulate the oxygen tension *in vivo* could be to optimize either the number of seeded algae in the implant or the intensity of light applied to the construct and assign them to meet the desired oxygen tension demanded by the tissue. Moreover, it is expected that the pO_2 will be substantially decreased *in vivo* by the metabolic consumption of oxygen by the surrounding cells, especially during wound healing where photosynthetic oxygen will be required to fulfill the hypermetabolic state of regenerating tissue.

No significant inflammatory response to *C. reinhardtii* was observed in two different *in vivo* models, evidencing that the presence of the microalgae does not cause major inflammation (Figs. 5B, 6 and 7). It is worth noting that although the athymic nude mice present a low T-cell-mediated response, the whole inflammatory cascade is fully functional in this model. In fact a high expression level of several inflammatory related molecules was observed in the scaffolds regardless of the group, showing also the importance of inflammation as a key mediator in tissue repair and regeneration [31]. The low response observed to the algae in mice might be partially explained by the seeding technique that includes an encapsulation step in fibrin, which has been shown to be effective in minimizing the host immune response [23]. The potential use of other encapsulation technologies to protect the engrafted photosynthetic cells *in vivo* remains to be explored in further settings. In order to look at the inflammatory response to *C. reinhardtii* in more detail, we decided to complement our study using a zebrafish model. This model was chosen because it presents a lower inflammatory background than a full-skin defect, which is intrinsically inflammatory, and also because it represents

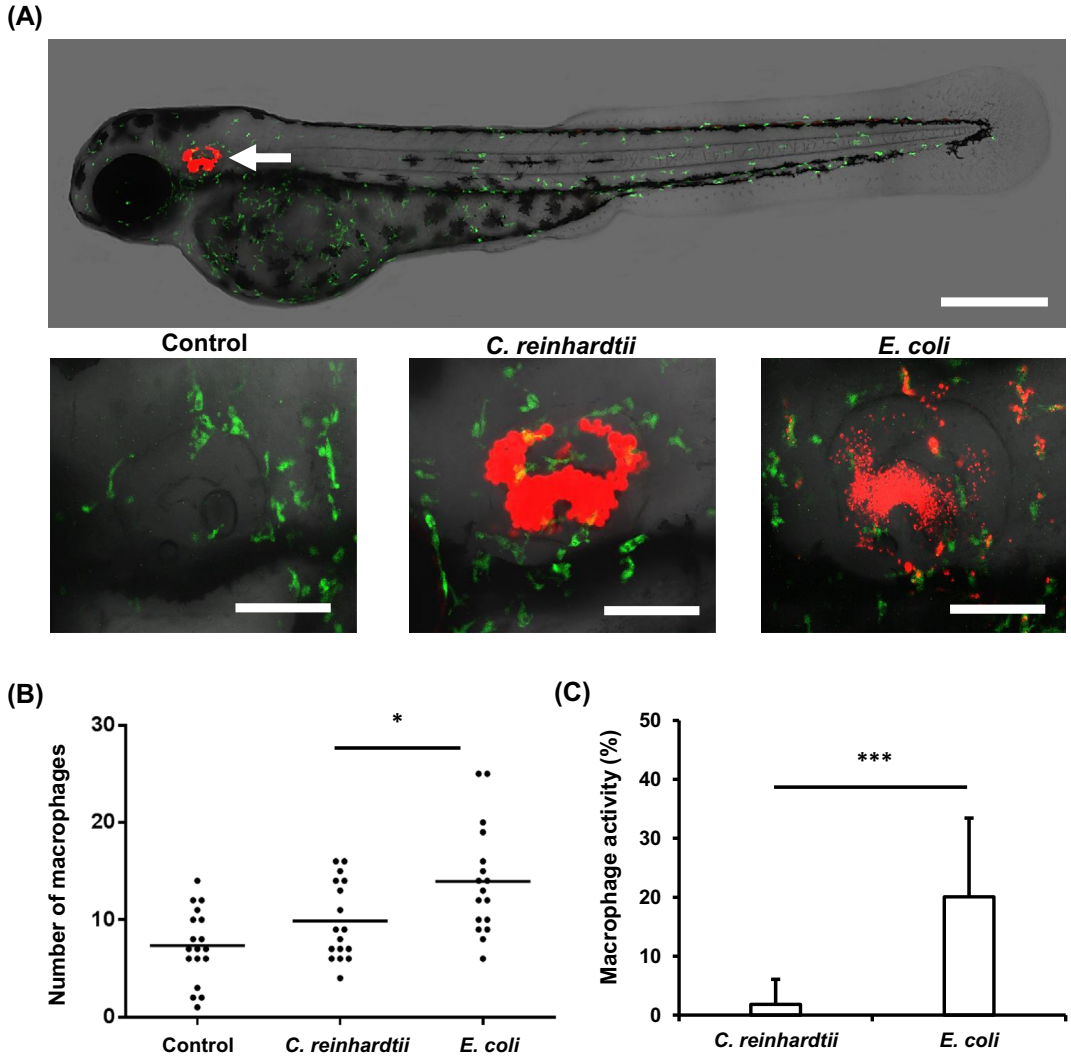

Fig. 7. Inflammatory response towards *C. reinhardtii* in a zebrafish model. *C. reinhardtii* was microinjected into the otic cavity of a zebrafish larvae expressing GFP in macrophages (A, upper), and the response against the algae was quantified and compared to *E. coli*-RFP (A, lower). In the injected area, the total number of macrophages (B) and the number of phagocytic macrophages (C) were significantly lower in *C. reinhardtii* when compared to *E. coli*. Scale bar represents 500 μm in A upper and 100 μm in A lower. $^{*}P \leqslant 0.05$, $^{***}P \leqslant 0.005$; $n \geqslant 3$. Results are shown as mean + SD.

an *in vivo* model where embryos of 3 days post-fertilization have developed fully mature phagocytic macrophages. Additionally, the optical transparency of the fish during the early juvenile stages allows the direct visualization of the cell–pathogen interactions in the living animal. Furthermore, the zebrafish otic cavity provides a unique and tractable model to study local inflammation induced by microorganisms because injection into this cavity is well tolerated by the fish and it keeps the defined antigen confined [32]. Making use of the availability of a transgenic lines expressing GFP in macrophages, it was possible to follow the interaction of these cells and *C. reinhardtii in vivo*. Although the zebrafish is not yet commonly used in the field of biomaterials, it has been extensively used in other research areas such as inflammation [33,34], wound repair [35] and tumor biology [36]. Similar results were observed in the mouse implant, where the algae seem to be intact and remain alive for at least 5 days after transplantation, generating chimeric algae–mammalian tissues *in vivo* (Fig. 5A).

Further research using non-immunocompromised animals, disease model organisms or critical size defects will give important insights into the potential applications of HULK in regenerative medicine. Above all, it would be interesting to evaluate HULK in the treatment of chronic wounds where it has been widely documented that lack of proper oxygen levels plays a key role [7] and oxygen therapies have been used to treat such patients [37]. One step further to engineer autotrophic tissues would be the use of genetically modified algae, which, in addition to oxygen, could also release other pro-regenerative bioactive substances such as growth factors, antibiotics, glucose or immunomodulatory molecules.

5. Conclusion

Photosynthetic scaffolds can be implanted in full-skin defects, generating chimeric tissues composed of mammalian and photosynthetic cells *in vivo*. In such tissues, photosynthetic cells survived for at least 5 days and did not trigger a significant innate immune response. Further studies in other clinically relevant animal models should be performed in order to evaluate the safety and efficiency of HULK for further uses in regenerative medicine.

Conflict of interest

The authors declare no conflicts of interest.

Acknowledgments

The authors would like to thank Dr. Ana Zuñiga for providing the *E.coli*-RFP strain. This work was partially financed by a CIRM-BMBF Early Translational II Award to J.T.E., ICGEB (CRP/CHI11-01) and the FONDAP Center for Genome regulation (Nr. 15090007) to both M.A. and J.T.E., and a DFG grant (Ni390/7-1) to J.N.

Appendix A. Figures with essential colour discrimination

Certain figures in this article, particularly Figs. 1–7, are difficult to interpret in black and white. The full colour images can be found in the on-line version, at http://dx.doi.org/10.1016/j.actbio.2014.12.012.

References

[1] Lutolf MP, Hubbell JA. Synthetic biomaterials as instructive extracellular microenvironments for morphogenesis in tissue engineering. Nat Biotechnol 2005;23:47–55.
[2] Priya SG, Jungvid H, Kumar A. Skin tissue engineering for tissue repair and regeneration. Tissue Eng Part B Rev 2008;14:105–18.
[3] Lutolf MP, Gilbert PM, Blau HM. Designing materials to direct stem-cell fate. Nature 2009;462:433–41.
[4] Hubbell JA, Thomas SN, Swartz MA. Materials engineering for immunomodulation. Nature 2009;462:449–60.
[5] Sen CK. Wound healing essentials: let there be oxygen. Wound Repair Regen 2009;17:1–18.
[6] Loenarz C, Schofield CJ. Physiological and biochemical aspects of hydroxylations and demethylations catalyzed by human 2-oxoglutarate oxygenases. Trends Biochem Sci 2011;36:7–18.
[7] Tandara AA, Mustoe TA. Oxygen in wound healing-more than a nutrient. World J Surg 2004;28:294–300.
[8] Rodriguez PG, Felix FN, Woodley DT, Shim EK. The role of oxygen in wound healing: a review of the literature. Dermatol Surg 2008;34:1159–69.
[9] Thom SR. Hyperbaric oxygen: its mechanisms and efficacy. Plast Reconstr Surg 2011;127:131–41.
[10] Eisenbud DE. Oxygen in wound healing: nutrient, antibiotic, signaling molecule, and therapeutic agent. Clin Plast Surg 2012;39:293–310.
[11] Dalton SJ et al. Mechanisms of chronic skin ulceration linking lactate, transforming growth factor-beta, vascular endothelial growth factor, collagen remodeling, collagen stability, and defective angiogenesis. J Invest Dermatol 2007;127:958–68.
[12] Dhall S et al. A novel model of chronic wounds: importance of redox imbalance and biofilm-forming bacteria for establishment of chronicity. PLoS ONE 2014;9(10):e109848.
[13] des Rieux A et al. 3D systems delivering VEGF to promote angiogenesis for tissue engineering. J Control Release 2011;150:272–8.
[14] Reckhenrich AK et al. Bioactivation of dermal scaffolds with a non-viral copolymer-protected gene vector. Biomaterials 2011;32:1996–2003.
[15] Asahara T, Kawamoto A, Masuda H. Concise review: circulating endothelial progenitor cells for vascular medicine. Stem Cells 2011;29:1650–5.
[16] Caplan AI. Why are MSCs therapeutic? New data: new insight. J Pathol 2009;217:318–24.
[17] Neupert J, Karcher D, Bock R. Generation of Chlamydomonas strains that efficiently express nuclear transgenes. Plant J 2009;57:1140–50.
[18] Harris EH. The Chlamydomonas sourcebook: introduction to Chlamydomonas and its laboratory use. Waltham, MA: Elsevier/Academic Press; 2009.
[19] Schenck TL, Chávez MN, Condurache AP, et al. A full skin defect model to evaluate vascularization of biomaterials in vivo. J Vis Exp 2014. http://dx.doi.org/10.3791/51428.
[20] Ellett F, Pase L, Hayman JW, Andrianopoulos A, Lieschke GJ. Mpeg1 promoter transgenes direct macrophage-lineage expression in zebrafish. Blood 2011;117:49–56.
[21] Shetty RP, Endy D, Knight Jr TF. Engineering BioBrick vectors from BioBrick parts. J Biol Eng 2008. http://dx.doi.org/10.1186/1754-1611-2-5.
[22] Hopfner U et al. Development of photosynthetic biomaterials for *in vitro* tissue engineering. Acta Biomater 2014;10(6):2712–7.
[23] Hunt NC, Grover LM. Cell encapsulation using biopolymer gels for regenerative medicine. Biotechnol Lett 2010;32:733–42.
[24] Malda J, Klein TJ, Upton Z. The roles of hypoxia in the in vitro engineering of tissues. Tissue Eng 2007;13:2153–62.
[25] Centis V, Vermette P. Enhancing oxygen solubility using hemoglobin- and perfluorocarbon-based carriers. Front Biosci 2009;14:665–88.
[26] Spahn DR. Current status of artificial oxygen carriers. Adv Drug Deliv Rev 2000;40:143–51.
[27] Chang TM. Hemoglobin-based red blood cell substitutes. Artif Organs 2004;28:789–94.
[28] Henkel-Honke T, Oleck M. Artificial oxygen carriers: a current review. AANA J 2007;75:205–11.
[29] Oh SH, Ward CL, Atala A, Yoo JJ, Harrison BS. Oxygen generating scaffolds for enhancing engineered tissue survival. Biomaterials 2009;30:757–62.
[30] Seifu DG, Isimjan TT, Mequanint K. Tissue engineering scaffolds containing embedded fluorinated-zeolite oxygen vectors. Acta Biomater 2011;7:3670–8.
[31] Eming SA, Krieg T, Davidson JM. Inflammation in wound repair: molecular and cellular mechanisms. J Invest Dermatol 2007;127:514–25.
[32] Benard EL et al. Infection of zebrafish embryos with intracellular bacterial pathogens. J Vis Exp 2012;61(e3781):1–8.
[33] Novoa B, Figueras A. Zebrafish: model for the study of inflammation and the innate immune response to infectious diseases. Adv Exp Med Biol 2012;946:253–75.
[34] Fang L, Miller YI. Emerging applications for zebrafish as a model organism to study oxidative mechanisms and their roles in inflammation and vascular accumulation of oxidized lipids. Free Radic Biol Med 2012;53(7):1411–20.
[35] Poss KD, Keating MT, Nechiporuk A. Tales of regeneration in zebrafish. Dev Dyn 2003;226(2):202–10 [Review].
[36] Moshal KS, Ferri-Lagneau KF, Leung T. Zebrafish model: worth considering in defining tumor angiogenesis. Trends Cardiovasc Med 2010;20:114–9.
[37] Kranke P, Bennett MH, Martyn-St James M, Schnabel A, Debus SE. Hyperbaric oxygen therapy for chronic wounds. Cochrane Database Syst Rev 2012;4:CD004123.